Plastic ablator and hydrodynamic instabilities: A first-principles set of microscopic coefficients

Flavien Lambert, Vanina Recoules

Plastic ablator and hydrodynamic instabilities: A first-principles set of microscopic coefficients

Flavien Lambert[1,*] and Vanina Recoules[1,2]
[1]*CEA, DAM, DIF, F-91297 Arpajon, France*
[2]*LUTH UMR8102, Observatoire de Paris, CNRS, Université Paris Diderot, 92195 Meudon, France*
(Received 26 June 2012; published 24 August 2012)

We have performed orbital-free and quantum molecular dynamics simulations on plastic ablator along two isochores, namely 7 and 9 $g\,cm^{-3}$, from 5 to 40 eV. These thermodynamic conditions correspond to those encountered during inertial confinement fusion capsule implosion when hydrodynamic instabilities can take place. The coupling between orbital-free and quantum approaches allowed us to compute an exhaustive set of microscopic coefficients, i.e., equation-of-state, ionic diffusion coefficients, thermal and electrical conductivities, spanning phenomena that can mitigate the growth of classical Rayleigh-Taylor instability. Comparisons to widely used models in hydrodynamics codes are developed.

DOI: 10.1103/PhysRevE.86.026405 PACS number(s): 52.25.Fi, 52.27.Gr, 52.65.Yy

I. INTRODUCTION

In the indirect drive scheme of inertial confinement fusion (ICF) [1], the fusible fuel, namely an equimolar mixture of deuterium and tritium, is brought into low temperature and high density through the use of an outer material called ablator whose role is to convert radiative energy—coming from the surrounding gold or uranium *hohlraum*—into mechanical work. Compression of the fuel is performed through a succession of finely tuned shock waves and a final implosion of the whole capsule that comes from the interaction between the outer ablation front and the centrifugal release wave born in the central gaseous fuel. The implosion should at the end of the process lead to the ignition of a small quantity of fuel that, then, should launch a nuclear combustion wave into the outer dense deuterium-tritium (DT) mixture.

Among the numerous phenomena that can prevent the capsule from igniting, i.e., generate a centrifugal thermonuclear combustion wave through the fuel, particular attention must be paid to hydrodynamic instabilities. One of the most deleterious is the classical Rayleigh-Taylor one that can exist at the ablator/fuel interface. This interface, due to fabrication processes, contains ripples that can, for some specific configurations, grow exponentially up to drilling the dense DT shell. The ripples can also be seeded by the instabilities on the outside ablation front by feed-through processes. To prevent these problems during the implosion phase, the ablator, pushing the fuel, must stay denser than the latter so that the interface stays hydrodynamically stable.

Apart from hard x rays coming from the M band of the *hohlraum* gold, the ablator at the interface is protected from the incoming radiation. Therefore, the behavior of the material—at the macroscopic level—is driven by hydrodynamics, thermal and species diffusion. All these phenomena require the knowledge of coefficients that are determined by the underlying microscopic physics: equation-of-state, shear viscosity, thermal conductivity and diffusion coefficients for the responses to, respectively, mechanical, heat, and concentration perturbations.

The current capsule designs for the Laser Mégajoule [2] and the National Ignition Facility [3] make use of a polyethylene ablator whose composition—when undoped—is close to C_2H_3. To conceive and predict the time evolution of capsules, designers use hydrodynamics codes that solve the fluid mechanics equations coupled to radiative energy transfer. Thermodynamical conditions relevant to the growth of hydrodynamics instabilities can be extracted from these numerical simulations. In the case of the Laser Mégajoule design, variations around the nominal capsule [4] showed that instabilities could grow for plastic at 7 $g\,cm^{-3}$, 30 eV, and, 9 $g\,cm^{-3}$, 10 eV in accordance with statement of Refs. [5,6].

The prime tool to study matter in this warm dense regime is quantum molecular dynamics (QMD) [7–9] but, as was explained in preceding publications [10], calculations are particularly difficult to perform when the electronic temperature become of the order of the Fermi one. Indeed, in QMD calculations, the one-body electronic states are populated through a Fermi-Dirac distribution so that high temperatures commonly involve a large number of orbitals. In a previous work [11,12], we circumvent this limitation by doing a two-step calculation:

(i) molecular dynamics is performed in the orbital-free scheme. Long runs allow to have access to structural properties—i.e., positions of the nuclei—as well as static (equation-of-state) and dynamical (diffusion coefficient, viscosity) properties;

(ii) a few nuclear positions are extracted from the previous simulations and are used as input for a complete quantum calculation to obtain electronic transport coefficients (thermal and electrical conductivities).

In this paper, we report the computation, by the same method, of the different coefficients along the two isochores from 5 to 40 eV.

After a brief description in Sec. II the theoretical and numerical features of quantum and orbital-free molecular dynamics, the evaluations of microscopic coefficients are presented in Sec. III, emphasizing the opportunity of using approximate models that can be implemented in hydrodynamics codes.

*flavien.lambert@cea.fr

II. ORBITAL-FREE AND QUANTUM MOLECULAR DYNAMICS

A. Theory overview

Both orbital-free [13–15] and quantum molecular dynamics rely on the adiabatic (Born-Oppenheimer) approximation [16]. The electrons are then acting on the nuclei as a many-body screening potential. Moreover, in the relevant thermodynamic conditions, the nuclear De Broglie wavelength is much smaller than the internuclei distance so that nuclei can be considered as classical particles. In the spirit of the Hohenberg-Kohn theorem [17] and the equivalent system of noninteracting particles of Kohn and Sham [18], the electronic free energy depends solely on the local electronic density n and reads as

$$F^e[n(\boldsymbol{r})] = F^0[n] + \frac{1}{2}\iint \mathrm{d}\boldsymbol{r}\mathrm{d}\boldsymbol{r}'\,\frac{n(\boldsymbol{r})n(\boldsymbol{r}')}{|\boldsymbol{r}-\boldsymbol{r}'|} - \sum_{\ell=1}^{\mathrm{N_a}} \mathcal{Z}_\ell \int \mathrm{d}\boldsymbol{r}'\,\frac{n(\boldsymbol{r}')}{|\boldsymbol{R}_\ell - \boldsymbol{r}'|} + \int \mathrm{d}\boldsymbol{r}\, f_{xc}[n], \quad (1)$$

where $F^0[n]$ and $f_{xc}[n]$ are, respectively, the kinetic-entropic and exchange-correlation parts.

In the "full" quantum case, the kinetic-entropic term is mapped into a system of noninteracting particles [19] represented by a set of orbitals and their respective eigenenergies, $\{|\psi_\ell\rangle, \varepsilon_\ell\}$, through

$$F^0[n] = \sum_\ell \left(f_\ell \int \mathrm{d}\boldsymbol{r}\,|\nabla\psi_\ell|^2 - \frac{1}{\beta}[f_\ell \ln f_\ell + (1-f_\ell)\ln(1-f_\ell)] \right), \quad (2)$$

where β is the inverse of the temperature and $f_\ell = f(\varepsilon_\ell)$ is the Fermi-Dirac distribution.

In the orbital-free world, the electronic free energy is approximated by a direct functional of the electronic density, in the true spirit of the Hohenberg-Kohn theorem, through a semiclassical expansion [20] of the Mermin functional, Eq. (2). The leading and next-to-leading order expansion, in terms of the Planck's constant, gives the well-known finite temperature Thomas-Fermi-von Weizsäcker model

$$F^0[n] = \frac{1}{\beta}\int \mathrm{d}\boldsymbol{r}\left(n(\boldsymbol{r})\Phi(n(\boldsymbol{r})) - \frac{2\sqrt{2}}{3\pi^2\beta^{\frac{3}{2}}} I_{\frac{3}{2}}[\Phi(n(\boldsymbol{r}))] \right) + \int \mathrm{d}\boldsymbol{r}\, h(n)\frac{|\nabla n(\boldsymbol{r})|^2}{n(\boldsymbol{r})}, \quad (3)$$

where the function h has a polynomial fit [21] and Φ is defined by

$$n(\boldsymbol{r}) = \frac{\sqrt{2}}{\pi^2\beta^{\frac{3}{2}}} I_{\frac{1}{2}}[\Phi(n(\boldsymbol{r}))]. \quad (4)$$

with I_ν the Fermi integral of degree ν.

B. Numerical features

The gradient correction in the orbital-free functional, Eq. (3), was only evaluated for equation-of-state purposes, Sec. III A. Its impact on transport coefficients was negligible in the thermodynamic regime of interest and within the statistical errors inherent to the method, Sec. III C. The exchange-correlation free energy f_{xc} was treated in the local density approximation [22] in orbital-free simulations and in the generalized-gradient approximation [23] in quantum calculations without taking into account any explicit temperature dependence [24].

The orbital-free simulations are performed with the OFMD code [13,25]. The 250 nuclei (100 carbon atoms and 150 hydrogen ones) were propagated in the isokinetic ensemble [26] during 50000 time steps after 5000 steps used for structure relaxation. The time step is chosen as a fraction of the plasma period [25]. Five snapshots of nuclear positions are extracted from the orbital-free calculations and are used for the full quantum simulation [11,12] carried out with the ABINIT [27] package.

III. MICROSCOPIC COEFFICIENTS

In this paragraph are shown the results of calculations coming either from orbital-free or quantum simulations. Comparisons are made to models that are or could be used in hydrodynamics codes providing a benchmark for microscopic coefficients.

A. Equation of state

Figure 1 presents the pressure versus temperature along the two isochores. Pressure is averaged on five different nuclear configurations. The average procedure performed over 5 or 50000 steps in the orbital-free simulations indicates that the values differ from less than a percent. Both orbital-free, with and without gradient correction, and quantum simulations are compared to the tabulated equation-of-state used in the nominal Laser Mégajoule capsule design. This latter is based on a modification of the quotidian equation of state (QEOS)

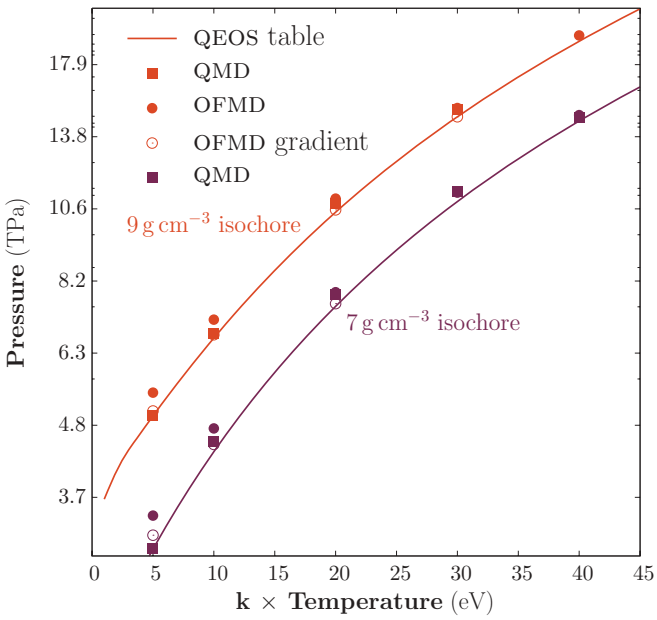

FIG. 1. (Color online) Pressure versus temperature along the two isochores obtained from quantum and orbital-free simulations as well as QEOS model.

model [28] where the thermal ionic part is replaced by the Yukawa results [29].

Except for the two lowest temperatures, the agreement between OFMD and QMD pressures is excellent, the difference being lower than 3%. The OFMD results are slightly lowered by a few Mbar by introducing the gradient correction allowing a better agreement between the two simulations at 5 and 10 eV in accordance with Ref. [30]. Furthermore, the agreement of the QEOS table over the entire range of temperature is excellent.

B. Effective ionization and coupling constant

Although ionization is not an observable, this notion is exhaustively used in plasma physics [31,32] and is often the free parameter in models of transport coefficients [33–38].

In orbital-free simulations, the charge of the nucleus is the atomic number, corresponding to an all-electron simulation. Consequently, OF calculations can be used to gauge the validity of prescription of both effective ionization and transport model. This procedure has already been used for pure elements [25,39,40], as well as for mixtures [15,41].

As previously described in Ref. [15], the OF average atom model (AAM) [42,43] can be used in conjunction with a mixing rule based on pressure matching [15,44] to provide the effective charge state. The results for both carbon and hydrogen are summarized in Table I. It is important to note that, when using a purely local functional (Thomas-Fermi + LDA exchange correlation), the pressure matching mixing rule is equivalent to equalize the free electron density of each element [13,15].

From the partial ionizations of Table I, several choices of average ionization of the mixture can be made. The first, labeled $\mathcal{Z}_1^\star$ comes straightforwardly from the pressure matching mixing rule, see Appendix,

$$\mathcal{Z}_1^\star = \sum_\ell x_\ell \mathcal{Z}_\ell^\star, \tag{5}$$

where x_ℓ are the atomic fractions. In the spirit of the ion-sphere model [45], another definition of average ionization, labeled

TABLE I. Effective charge states $\mathcal{Z}_i^\star$ and partial density ρ_i of carbon and hydrogen inside the plasma obtained by coupling the OF average atom model and a mixing rule based on pressure matching.

ρ ($\mathrm{g\,cm^{-3}}$)	kT_e (eV)	$\mathcal{Z}_\mathrm{C}^\star$	ρ_C ($\mathrm{g\,cm^{-3}}$)	$\mathcal{Z}_\mathrm{H}^\star$	ρ_H ($\mathrm{g\,cm^{-3}}$)
9	5	2.77	11.26	0.75	3.45
	10	2.79	11.25	0.76	3.46
	20	2.89	11.22	0.77	3.49
	30	3.03	11.16	0.80	3.54
	40	3.18	11.09	0.82	3.59
7	5	2.59	8.85	0.73	2.62
	10	2.62	8.84	0.74	2.62
	20	2.77	8.80	0.76	2.66
	30	2.94	8.73	0.79	2.70
	40	3.12	8.67	0.82	2.76

TABLE II. Effective charge calculated from the average atom model.

ρ	kT_e	$\mathcal{Z}_1^\star$	$\mathcal{Z}_2^\star$	$\mathcal{Z}_3^\star$
9	5	1.56	1.68	1.90
	10	1.57	1.70	1.91
	20	1.62	1.75	1.95
	30	1.69	1.83	2.01
	40	1.76	1.91	2.07
7	5	1.47	1.59	1.83
	10	1.49	1.61	1.85
	20	1.56	1.69	1.90
	30	1.65	1.78	1.97
	40	1.74	1.88	2.05

$\mathcal{Z}_2^\star$, can be defined as

$$\mathcal{Z}_2^\star = \sqrt{\sum_n x_n (\mathcal{Z}_n^\star)^{\frac{1}{3}} \times \sum_\ell x_\ell (\mathcal{Z}_\ell^\star)^{\frac{5}{3}}}. \tag{6}$$

Finally, as done in many hydrodynamics codes—since this procedure is the fastest—an average element defined as $\mathcal{Z} = \sum_\ell x_\ell \mathcal{Z}_\ell$ and $\mathcal{A} = \sum_\ell x_\ell \mathcal{A}_\ell$ (3 and 5.4, respectively, for C_2H_3) can be introduced in the AAM to get an evaluation of effective charge state, labeled $\mathcal{Z}_3^\star$.

The different values are reported in Table II.

For all temperatures, $\mathcal{Z}_2^\star$ and $\mathcal{Z}_3^\star$ are greater than $\mathcal{Z}_1^\star$ by, respectively, 10 and 20 %. From the different values of ionization can be calculated an effective coupling constant of the plasma through

$$\Gamma^\star = \left(\frac{3}{4\pi}\right)^{\frac{1}{3}} \frac{\mathcal{Z}^{\star 2}}{n^{\frac{1}{3}} kT}, \tag{7}$$

with n the number density.

The third definition of ionization always provide a higher coupling constant but the order of magnitude stays the same. The coupling constant as well as the average charge state—which are not straightforwardly defined in mixtures—are nevertheless key ingredients in describing plasma behavior and in models, like the one component plasma [46]. It allows to compute easily but approximately some transport coefficients like viscosity [34] or diffusion coefficient [33], see Sec. III C. Considering the "limited" differences between the choices of ionizations, the impact on transport coefficients is lower than the precision required by using these coefficients in hydrodynamics codes.

C. Dynamical properties

Both ionic self-diffusion D_ℓ, interdiffusion D_HC and shear viscosity η are obtained through correlation functions.

The self-diffusion coefficient is calculated from the nuclear velocities,

$$D_\ell = \frac{1}{\beta \mathcal{M}_\ell} \int_{\mathbb{R}^+} \frac{\langle \boldsymbol{v}_\ell(t) \cdot \boldsymbol{v}_\ell(0) \rangle}{\langle \boldsymbol{v}_\ell(0) \cdot \boldsymbol{v}_\ell(0) \rangle} \mathrm{d}t, \tag{8}$$

$\boldsymbol{v}_\ell$, and $\mathcal{M}_\ell$ being, respectively, the velocity and the mass of an atom of specie ℓ.

From the current [47] is evaluated the interdiffusion coefficient through

$$D_{\mathrm{HC}} = \frac{g}{\beta}\frac{x_{\mathrm{H}}\mathcal{M}_{\mathrm{H}} + x_{\mathrm{C}}\mathcal{M}_{\mathrm{C}}}{\mathcal{M}_{\mathrm{H}}\mathcal{M}_{\mathrm{C}}}\int_{\mathbb{R}^+}\frac{\langle \boldsymbol{j}(t)\cdot\boldsymbol{j}(0)\rangle}{\langle \boldsymbol{j}(0)\cdot\boldsymbol{j}(0)\rangle}\,\mathrm{d}t, \tag{9}$$

with

$$\boldsymbol{j} = x_{\mathrm{C}}\sum_{\ell\in\mathrm{H}}\boldsymbol{v}_\ell - x_{\mathrm{H}}\sum_{\ell\in\mathrm{C}}\boldsymbol{v}_\ell \tag{10}$$

and g a thermodynamic factor taken equal to 1.

The shear viscosity is computed from the off-diagonal elements of the microscopic stress tensor $\varsigma^{\mu\nu}$,

$$\eta = \frac{\beta}{\Omega}\int_{\mathbb{R}^+}\langle\varsigma^{\mu\nu}(t)\varsigma^{\mu\nu}(0)\rangle\,\mathrm{d}t, \tag{11}$$

with Ω the volume of the system.[1] It is important to note that, in the case of OFMD, the stress tensor contains nuclear [48] and electronic [49,50] contributions.

Since the self-diffusion coefficient is averaged over the particles, convergence is reached much faster than for interdiffusion coefficient and viscosity. Considering the number of time steps involved in OFMD simulations, the self-diffusion coefficients are obtained within less than 5% error whereas the two others are evaluated within an error of 20% [51].

1. Diffusion coefficients

In recent studies [52], species separation due to barodiffusion, i.e., diffusion driven by pressure gradients, has been brought to light as a potential threat to ignition since it modifies drastically the properties of the ablator material. In order to model and simulate such a phenomena in hydrodynamics codes, the knowledge of the self-diffusion coefficient of each species *inside the mixture* and the interdiffusion is required. These quantities are given in molecular dynamics simulations through Eqs. (8) and (9). Table IV records the diffusion coefficients along the two isochores. It should be noted that these coefficients are a direct output of OFMD simulations that are particularly computationally efficient in comparison to its orbital-based counterpart. Therefore these techniques could be used in thermodynamic conditions not restricted to the two isochores of this paper, providing the diffusion coefficients for the entire thermodynamics path followed by the ablator.

The comparison between the computed interdiffusion coefficient and the linear mixing [34,47] is very good. Equation (9) shows that, since $x_{\mathrm{C}}\mathcal{M}_{\mathrm{C}} \gg x_{\mathrm{H}}\mathcal{M}_{\mathrm{H}}$, the factor in front of the correlation function reduces to $x_{\mathrm{C}}/\mathcal{M}_{\mathrm{H}}$. Furthermore, hydrogen at a given temperature has a behavior much more "kinetic" than carbon so that the hydrogen velocities are greater than the carbon ones and stay correlated longer. Therefore, the terms involving carbon velocities can be, as a first approximation, neglected. Eq. (9) is then rewritten $x_{\mathrm{C}}D_{\mathrm{H}}$, explaining the behavior of Table IV. The interdiffusion coefficient is dominated by the light element.

2. Shear viscosity

Transition from laminar to turbulent flow is also a key question on NIF since doping material inside the fuel at the end of the implosion phase is experimentally characterized for several MJ experiments [53]. The purpose of this paragraph is to provide a rule of thumb to evaluate rapidly the order of magnitude of the viscosity so that designers would be able to characterize the state of the plasma in terms of Reynolds number.

As previously stated, the one component plasma (OCP) is a key model used in the plasma community since most of its properties depends only on the coupling constant of the system and fits obtained from numerical simulations are available either for equation of state [46] or transport coefficients [34]. In a previous work, comparisons had been made on the viscosity of a D/Cu mixture between a direct calculation of the viscosity by OFMD and a mixing rule based on OCP [15]. The model, in the following paragraph, is slightly different and simpler. OFMD viscosity is compared to the OCP one, Fig. 2, evaluated for an hypothetical plasma whose coupling constant is $\Gamma_2^\star$, Table III. This rule was already used for a deuterium-tritium mixture [41] and the conclusions drawn stay valid in our plastic case.

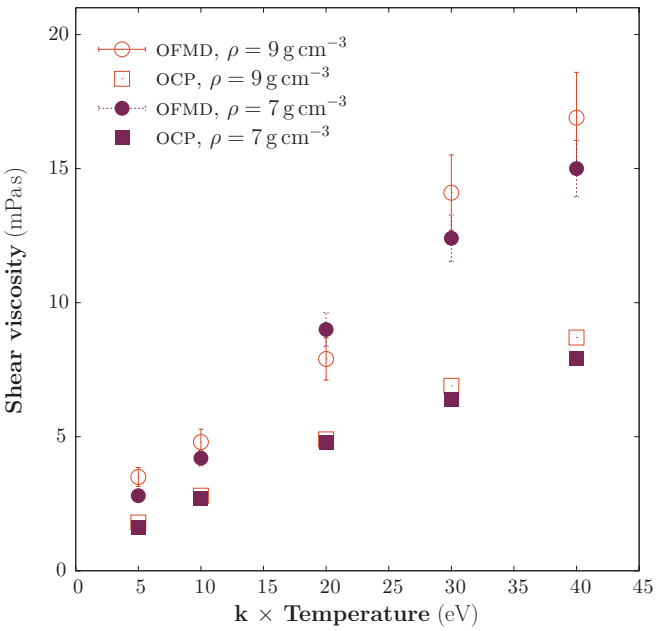

FIG. 2. (Color online) Shear viscosity obtained from the OFMD simulations and the OCP fit from Ref. [34] using the effective coupling constant $\Gamma_2^\star$ of Table III.

TABLE III. Effective coupling constant calculated from effective charges of Table I.

ρ	kT_e	$\Gamma_1^\star$	$\Gamma_2^\star$	$\Gamma_3^\star$
9	5	11.3	13.2	16.9
	10	5.7	6.7	8.5
	20	3.1	3.6	4.4
	30	2.2	2.6	3.2
	40	1.8	2.1	2.5
7	5	9.3	10.8	14.4
	10	4.8	5.5	7.3
	20	2.6	3.0	3.9
	30	1.9	2.3	2.8
	40	1.6	1.9	2.2

[1]This formulation is valid for a stationary and uniform fluid.

TABLE IV. Self- and interdiffusion coefficients extracted from OFMD simulations. The interdiffusion is compared to a linear mixing of self-diffusion coefficient.

ρ (g cm^{-3})	kT_e (eV)	D_H	D_C	D_{HC} (10^{-3}cm^2 s^{-1})	$x_C D_H + x_H D_C$
9	5	9.6	2.6	6	5.4
	10	23.1	4.9	14	12.2
	20	57.7	9.3	31	28.7
	30	96.8	13.3	55	46.7
	40	140.4	18.0	76	67.0
7	5	11.8	3.1	7	6.6
	10	28.5	5.8	17	14.9
	20	70.4	11.3	37	34.9
	30	121.8	16.5	55	58.6
	40	174.1	22.0	94	82.8

Although the effective OCP results underestimate the OFMD viscosity by a factor of 2, the simple rule allows to obtain the right trend in terms of dependency on both density and temperature.

D. Electronic transport coefficients

As explained in the previous paragraphs, OF methods are based on eliminating the Kohn-Sham orbitals in computing the electronic free energy by using a direct approximation of the latter. Despite its accuracy in calculating the equation of state, this technique presents a serious drawback when dealing with electronic transport coefficient. Indeed, most of the transport coefficients are expressed in terms of scattering cross sections, i.e., transitions between many-body electronic states which, in the case of one-body equivalent system like the Kohn-Sham theory, can be mapped into transitions between single-electron quantum states. Therefore, OF techniques, dealing only with the local electronic density, are not well suited to tackle such problems.

On the other hand, mean field quantum methods, like the Kohn-Sham scheme for example, have proved to be well suited to evaluate electronic coefficients, like electrical [7,54,55] and thermal [9,56] conductivities. Indeed, with the notations of Sec. II, linear response theory from Kubo and Greenwood [57, 58] leads to the following expression for the elastic scattering cross section:

$$s(\varepsilon) = \frac{1}{\Omega} \sum_{\ell,\ell'} \sum_{\alpha} |\langle \psi_{\ell'}| v_\alpha |\psi_\ell\rangle|^2 \delta(\varepsilon_{\ell'} - \varepsilon)\delta(\varepsilon_\ell - \varepsilon), \quad (12)$$

where ε is the electron energy, Ω stands for the volume of the system and v_α is the α component of the velocity operator. Although, in the Kohn-Sham theory, one body quantum states are only mathematical tools to obtain the local electronic density, they can be successfully introduced as $\{|\psi_\ell\rangle, \varepsilon_\ell\}$ in Eq. (12) as was shown by comparison to experiments, see for example [54,55,59,60]. The generic Onsager kinetic coefficients can be computed from the scattering cross section $s(\varepsilon)$,

$$\mathcal{L}_{ij} = (-1)^{i+j+1} \int \mathrm{d}\varepsilon \, \frac{\partial f(\varepsilon,\mu)}{\partial \varepsilon} (\varepsilon - \mu)^{i+j-2} s(\varepsilon), \quad (13)$$

with f the Fermi-Dirac distribution and μ the chemical potential from which the electronic transport coefficients [61] are evaluated, namely the electrical conductivity

$$\sigma = \mathcal{L}_{11}, \quad (14)$$

and the thermal conductivity

$$\kappa = \frac{1}{T}\left(\mathcal{L}_{22} - \frac{\mathcal{L}_{12} \times \mathcal{L}_{21}}{\mathcal{L}_{11}}\right). \quad (15)$$

By using the properties of the Dirac functions, Eq. (13) can be rewritten as [62]

$$\begin{aligned}\mathcal{L}_{ij} = (-1)^{(i+j)} \frac{1}{\Omega} \lim_{\Delta\varepsilon\to 0} \sum_{\boldsymbol{k}} W(\boldsymbol{k}) \\ \times \sum_{\ell,\ell'} \sum_{\alpha} \frac{f\left(\varepsilon_{\ell'}^{\boldsymbol{k}}\right) - f\left(\varepsilon_{\ell}^{\boldsymbol{k}}\right)}{\varepsilon_{\ell'}^{\boldsymbol{k}} - \varepsilon_{\ell}^{\boldsymbol{k}}} \left(\varepsilon_{\ell'}^{\boldsymbol{k}} - \mu\right)^{i-1} \left(\varepsilon_{\ell}^{\boldsymbol{k}} - \mu\right)^{j-1} \\ \times \left|\left\langle \psi_{\ell'}^{\boldsymbol{k}}\right| v_\alpha \left|\psi_{\ell}^{\boldsymbol{k}}\right\rangle\right|^2 \delta\left(\varepsilon_{\ell'}^{\boldsymbol{k}} - \varepsilon_{\ell}^{\boldsymbol{k}} - \Delta\varepsilon\right). \quad (16)\end{aligned}$$

Equations (14) and (15) are applied to the energy dependent form of the kinetic coefficient. Then, by extrapolating to zero energy, electrical and thermal conductivities are obtained. It is important to note that the previous derivation of the transport coefficients is valid for *a given static nuclear configuration* and, consequently, an average must be done over several configurations to be representative of the nuclear structure, which is disordered in the case of the plasmas we are dealing with. The probability density used is the Maxwell-Boltzmann one, since in our Born-Oppenheimer approximation (Sec. II), the nuclei are treated as classical particles. Nevertheless, calculations show a weak dependence of the thermal conductivities on the nuclear structure.

The quantum calculations were performed with up to 6000 bands for the highest temperatures which correspond to a thermal occupancy of 10^{-4}.

The QMD thermal conductivities along the two isochores are presented in Figs. 3 and 4. Comparisons are performed to models used in either ICF or astrophysics, namely Hubbard-Spitzer [35,63] and Ichimaru [36]. These models have been developed for single element and, consequently, an additional mixing rule has to be exhibited to compute the thermal conductivities for a multispecies material like plastic. Two choices can be made:

(i) define an average material, mixture of H and C, through effective atomic number and mass and compute the thermal conductivity of this average element. This procedure is used in hydrodynamics codes for ICF;

(ii) compute conductivities of H and C, requiring partial densities as an input, and mix the conductivities.

The two methods have been tested and are plotted on Fig. 3. We have defined an average plastic element whose atomic mass is 3.5 and effective ionization is determined by $\mathcal{Z}_3^\star$, Table I (labeled Hubbard-Spitzer, orange line) or by the pressure-matching mixing rule, $\mathcal{Z}_1^\star$ (labeled Hubbard-Spitzer $\mathcal{Z}_1^\star$, orange dots, or Ichimaru $\mathcal{Z}_1^\star$, purple dots). In the case of mixing conductivities, we have used a Faber-Ziman like mixing rule [6] in conjunction with the pressure matching mixing rule for determining partial densities (white dots).

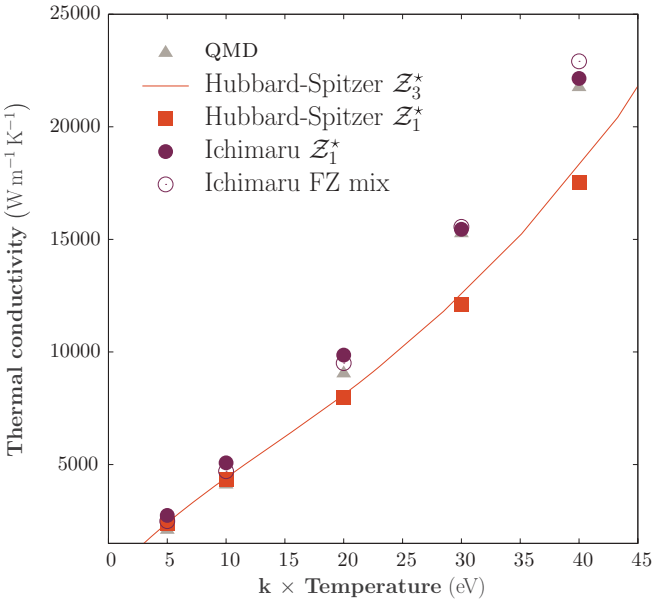

FIG. 3. (Color online) Thermal conductivities along the 7 g cm^{-3} isochore from QMD simulations and various models coupled to mixing rules.

As can be seen on Fig. 3, the choice of ionization—Hubbard-Spitzer $\mathcal{Z}_1^\star$ and $\mathcal{Z}_3^\star$—does not generate important modifications on the conductivities. Let us recall here that the Hubbard-Spitzer model is in fact composed of two models, the Hubbard one that was developed for degenerate plasmas and the Spitzer one that is well suited for the kinetic regime. The total thermal conductivity is computed by a quadratic mean of the two aforementioned conductivities. In the regime studied in this paper, both conductivities play a role in the total one

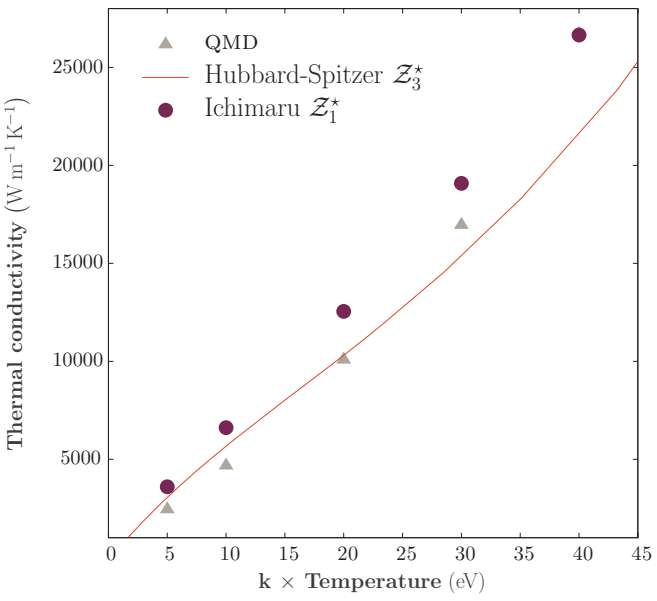

FIG. 4. (Color online) Thermal conductivities along the 9 g cm^{-3} isochore from QMD simulations and various models coupled to mixing rules.

so that the QMD calculations allow to check the transition between the two models.

The Ichimaru's values, with the two methods previously defined, are always greater than the Hubbard-Spitzer ones and are close whatever the method of mixing. The agreement between Ichimaru's model and QMD is good except at low temperatures where QMD provide lower conductivities. Nevertheless, the trend in temperature is correctly reproduced by all the models and a quantitative agreement of 10% with QMD at intermediate temperature is reached which is highly sufficient considering other sources of errors in hydrodynamics simulations.

IV. CONCLUSION

We have performed first-principles simulations to compute a complete set of microscopic coefficients for plastic in a regime relevant to hydrodynamic instabilities of ICF capsules. It has been shown that the QEOS recovers the QMD results and that conductivity models with a suitable choice of ionization provide results in good agreement with linear-response theory. Rules of thumb for other transport coefficients have been also exhibited.

ACKNOWLEDGMENTS

The authors would like to thank Gwenael Salin for providing the QEOS table as well as Alain Decoster and Jean Clérouin for the computation of the conductivity models.

APPENDIX : AVERAGE CHARGE STATE OF THE PLASMA WITH THE PRESSURE MATCHING MIXING RULE

The plasma is represented by the total volume Ω and number of nuclei N, defining the number density by $n = N/\Omega$. The effective free electron number is labeled $N^{e\star}$ so that the average effective charge state is written $\mathcal{Z}^\star = N^{e\star}/N$.

If the partial quantities associated with each element in the mixture are labeled ℓ with the previous notation, the pressure matching mixing rule states

$$p_\ell = p_{\ell'}, \forall\, \ell, \ell' \tag{A1}$$

and

$$\Omega = \sum_\ell \Omega_\ell \leftrightarrow \frac{1}{n} = \sum_\ell \frac{x_\ell}{n_\ell}, \tag{A2}$$

where p_ℓ and x_ℓ are the partial pressure and atomic fraction of element ℓ. It can be shown [15] that the pressure of the system is in fact p_ℓ.

In the context of a purely local functional, the pressure obtained with the orbital-free average atom model depends solely on the free electron density. Consequently, the mixing rule can be expressed as

$$n_\ell^{e\star} = n_{\ell'}^{e\star} = n^{e\star}, \forall\, \ell, \ell' \tag{A3}$$

with $n_\ell^{e\star}$ the partial free electronic density of element ℓ.

From Eq. (A3), the total number of free electron can be written

$$N^{e\star} = \sum_\ell n_\ell^{e\star}\Omega_\ell = n^{e\star}\Omega, \tag{A4}$$

so that the common value $n^{e\star}$ is indeed the total free electron density. The effective charge state reads therefore as

$$\mathcal{Z}^\star = \frac{n^{e\star}}{n} = \sum_\ell \frac{x_\ell n^{e\star}}{n_\ell} = \sum_\ell x_\ell \mathcal{Z}_\ell^\star. \tag{A5}$$

[1] R. P. Drake, *High-Energy-Density Physics: Fundamentals, Inertial Fusion, and Experimental Astrophysics (Shock Wave and High Pressure Phenomena)* (Springer, Berlin, 2006).
[2] LMJ project, http://www-lmj.cea.fr/.
[3] NIF project, https://lasers.llnl.gov/.
[4] S. Laffite and P. Loiseau, Phys. Plasmas **17**, 102704 (2010).
[5] B. A. Hammel, S. W. Haan, D. S. Clark, M. J. Edwards, S. H. Langer, M. M. Marinak, M. V. Patel, J. D. Salmonson, and H. A. Scott, High Energy Density Phys. **6**, 171 (2010).
[6] D. E. Hanson, L. A. Collins, J. D. Kress, and M. P. Desjarlais, Phys. Plasmas **18**, 082704 (2011).
[7] L. A. Collins, S. R. Bickham, J. D. Kress, S. Mazevet, T. J. Lenosky, N. J. Troullier, and W. Windl, Phys. Rev. B **63**, 184110 (2001).
[8] M. P. Desjarlais, Phys. Rev. B **68**, 064204 (2003).
[9] B. Holst, R. Redmer, and M. P. Desjarlais, Phys. Rev. B **77**, 184201 (2008).
[10] S. Mazevet, F. Lambert, F. Bottin, G. Zérah, and J. Clérouin, Phys. Rev. E **75**, 056404 (2007).
[11] V. Recoules, F. Lambert, A. Decoster, B. Canaud, and J. Clerouin, Phys. Rev. Lett. **102**, 075002 (2009).
[12] F. Lambert, V. Recoules, A. Decoster, J. Clerouin, and M. Desjarlais, Phys. Plasmas **18**, 056306 (2011).
[13] F. Lambert, Ph.D. thesis, Université Paris XI - Commissariat à l'Énergie Atomique (2007), http://tel.archives-ouvertes.fr/tel-00167424/fr/.
[14] F. Lambert, J. Clérouin, and G. Zérah, Phys. Rev. E **73**, 016403 (2006).
[15] F. Lambert, J. Clérouin, J. F. Danel, L. Kazandjian, and G. Zérah, Phys. Rev. E **77**, 026402 (2008).
[16] R. Balian, *From Microphysics to Macrophysics: Methods and Applications of Statistical Physics* (Springer-Verlag, Berlin and Heidelberg, 2006).
[17] P. Hohenberg and W. Kohn, Phys. Rev. B **136**, B864 (1964).
[18] W. Kohn and L. J. Sham, Phys. Rev. **140**, 1133 (1965).
[19] N. D. Mermin, Phys. Rev. **137**, 1441 (1965).
[20] M. Brack and R. K. Bhaduri, *Semiclassical Physics* (Westview Press, Boulder, 2003).
[21] F. Perrot, Phys. Rev. A **20**, 586 (1979).
[22] J. P. Perdew and A. Zunger, Phys. Rev. B **23**, 5048 (1981).
[23] J. P. Perdew, K. Burke, and M. Ernzerhof, Phys. Rev. Lett. **77**, 3865 (1996).
[24] J. F. Danel, L. Kazandjian, and G. Zérah, Phys. Plasmas **13**, 092701 (2006).
[25] F. Lambert, J. Clérouin, and S. Mazevet, Europhys. Lett. **75**, 681 (2006).
[26] P. Minary, G. J. Martyna, and M. E. Tuckerman, J. Chem. Phys. **118**, 2527 (2003).
[27] X. Gonze, B. Amadon, P. M. Anglade, J. M. Beuken, F. Bottin, P. Boulanger, F. Bruneval, D. Caliste, R. Caracas, M. Cote *et al.*, Comput. Phys. Commun. **180**, 2582 (2009).
[28] R. M. More, K. H. Warren, D. A. Young, and G. B. Zimmerman, Phys. Fluids **31**, 3059 (1988).
[29] D. Gilles, F. Lambert, J. Clérouin, and G. Salin, High Energy Density Physics **3**, 95 (2007).
[30] J. F. Danel, L. Kazandjian, and G. Zérah, Phys. Plasmas **15**, 072704 (2008).
[31] S. Ichimaru, H. Iyetomi, and S. Tanaka, Phys. Rep. **149**, 91 (1987).
[32] S. Ichimaru, Rev. Mod. Phys. **54**, 1017 (1982).
[33] J. Daligault, Phys. Rev. Lett. **96**, 065003 (2006).
[34] S. Bastea, Phys. Rev. E **71**, 056405 (2005).
[35] L. Spitzer and R. Harm, Phys. Rev. **89**, 977 (1953).
[36] H. Kitamura and S. Ichimaru, Phys. Rev. E **51**, 6004 (1995).
[37] H. Minoo, C. Deutsch, and J. P. Hansen, Phys. Rev. A **14**, 840 (1976).
[38] H. Minoo, C. Deutsch, and J. P. Hansen, J. Phys. Lett.-Paris **38**, L191 (1977).
[39] J. D. Kress, J. S. Cohen, D. P. Kilcrease, D. A. Horner, and L. A. Collins, High Energy Density Phys. **7**, 155 (2011).
[40] J. D. Kress, J. S. Cohen, D. P. Kilcrease, D. A. Horner, and L. A. Collins, Phys. Rev. E **83**, 026404 (2011).
[41] J. D. Kress, J. S. Cohen, D. A. Horner, F. Lambert, and L. A. Collins, Phys. Rev. E **82**, 036404 (2010).
[42] R. P. Feynman, N. Metropolis, and E. Teller, Phys. Rev. **75**, 1561 (1949).
[43] W. R. Johnson, FORTRAN program for temperature-dependent thomas-fermi atom (2002), http://www.nd.edu/∼johnson/.
[44] J. F. Danel, L. Kazandjian, and G. Zerah, Phys. Rev. E **79**, 066408 (2009).
[45] J. P. Hansen, G. M. Torrie, and P. Vieillefosse, Phys. Rev. A **16**, 2153 (1977).
[46] M. Baus and J. P. Hansen, Phys. Rep. **59**, 2 (1980).
[47] D. B. Boercker and E. L. Pollock, Phys. Rev. A **36**, 1779 (1987).
[48] B. Bernu and P. Vieillefosse, Phys. Rev. A **18**, 2345 (1978).
[49] O. H. Nielsen and R. M. Martin, Phys. Rev. B **32**, 3780 (1985).
[50] A. DalCorso and R. Resta, Phys. Rev. B **50**, 4327 (1994).
[51] J.-F. Danel, L. Kazandjian, and G. Zérah, Phys. Rev. E **85**, 066701 (2012).
[52] P. Amendt, S. C. Wilks, C. Bellei, C. K. Li, and R. D. Petrasso, Phys. Plasmas **18**, 056308 (2011).
[53] S. P. Regan, R. Epstein, B. A. Hammel, L. J. Suter, J. Ralph, H. Scott, M. A. Barrios, D. K. Bradley, D. A. Callahan, C. Cerjan *et al.*, Phys. Plasmas **19**, 056307 (2012).
[54] M. P. Desjarlais, J. D. Kress, and L. A. Collins, Phys. Rev. E **66**, 025401 (2002).
[55] P. Renaudin, V. Recoules, P. Noiret, and J. Clerouin, Phys. Rev. E **73**, 056403 (2006).
[56] V. Recoules and J. P. Crocombette, Phys. Rev. B **72**, 104202 (2005).

[57] R. Kubo, J. Phys. Soc. Jpn. **12**, 570 (1957).
[58] D. A. Greenwood, Proc. Phys. Soc. London **71**, 585 (1958).
[59] J. Clerouin, V. Recoules, S. Mazevet, P. Noiret, and P. Renaudin, Phys. Rev. B **76**, 064204 (2007).
[60] J. Clerouin, P. Noiret, V. N. Korobenko, and A. D. Rakhel, Phys. Rev. B **78**, 224203 (2008).
[61] G. V. Chester and A. Thellung, Proc. Phys. Soc. London **77**, 1005 (1961).
[62] S. Mazevet, M. Torrent, V. Recoules, and F. Jollet, High Energy Density Phys. **6**, 84 (2010).
[63] W. B. Hubbard and M. Lampe, Astrophys. J. Suppl. Ser. **18**, 297 (1969).